International Journal of Fatigue 209 (2026) 109620

Contents lists available at ScienceDirect

International Journal of Fatigue

journal homepage: www.elsevier.com/locate/ijfatigue

Grinding – good or bad for reduction of rolling contact fatigue–observations from in-service rails with white etching layer

Tim Vernaillen [a,b], Pan Zhang [a,*], Stefan Lundström Sveder [c], Alfredo Núñez [a], Rolf Dollevoet [a], Zili Li [a,*]

[a] Delft University of Technology, Stevinweg 1, 2628CN Delft, The Netherlands
[b] Infrabel, Place Marcel Broodthaers 2, 1060 Brussels, Belgium
[c] Trafikverket, Röda Vägen, 1781 89 Borlänge, Sweden

ARTICLE INFO

Keywords:
Rail rolling contact fatigue
Rail grinding
Microstructural analysis
White etching layer
Ratcheting

ABSTRACT

Rail grinding has been widely applied in railway networks worldwide to remove or prevent rolling contact fatigue (RCF) cracks. However, some concerns have arisen regarding grinding, that it may introduce initial damage to the rail and largely shorten the RCF life. This work aims to better understand the effect of grinding on the long-term degradation of in-service rails, particularly concerning White Etching Layer (WEL) and RCF cracks. Seven rail samples were selected and taken from the Belgian and Swedish railway networks, with different grinding histories, accumulated loads, and steel grades. The mechanical and microstructural properties of these samples were examined through the hardness test and optical microscopy. WEL and microcracks were observed in both ground and non-ground rails, suggesting that rail grinding does not create additional defects nor negatively impact the rail surface after long-term service. Macrocracks were observed only in rail samples that had undergone zero or a single grinding cycle, confirming the beneficial role of rail grinding in mitigating RCF cracks. Ratcheting is the dominant crack initiation mechanism under the examined conditions, while WEL may also contribute to crack formation, given that macrocracks predominantly occur at the transition between the WEL and the pearlite.

1. Introduction

Rolling contact fatigue (RCF) has been a significant and growing problem in rail networks worldwide [1], especially since the early 2000 s, largely driven by advancements in modern rolling stock. RCF is induced by repeated high-stress wheel–rail contact, leading to the progressive loss of ductility in rail materials and the initiation of surface or subsurface cracks [2–4]. These cracks may propagate under consecutive cyclic loading, sometimes with fluid entrapment [5,6], extend deeper into the rail, resulting in catastrophic rail breakage [7,8]. With increasing axle loads, train speeds and traffic density, the risk posed by RCF continues to rise, becoming a serious threat to rail safety. Therefore, timely and effective measures for RCF mitigation and prevention are essential to ensure safe and reliable railway operations.

Rail grinding has been widely implemented in the railway industry to restore the railhead profile and remove surface defects such as corrugation [9,10] and RCF cracks [11]. Today, it is globally employed as a standard preventive maintenance practice aimed at mitigating RCF by removing a thin surface layer of material that typically contains plastically deformed microstructures and early-stage cracks [1]. Despite variations in grinding depth and interval across different rail networks, the positive impact of rail grinding on extending rail service life and reducing maintenance costs has been well documented [12–14]. However, concerns have also been raised regarding potential adverse effects on the surface integrity of rails [15], particularly when grinding parameters are not properly controlled [16].

One of the primary concerns regarding rail grinding is its potential to induce initial damage to the rail surface due to the high friction and temperature rise (e.g., above 800 °C [17,18]). A study of RCF in a head-hardened rail [19] reported that a White Etching Layer (WEL) with a depth up to 8 μm was identified in the low rail after just 1 million gross tonnes (MGT) of service, likely resulting from grinding operations. WEL is a typical microstructural phenomenon in rail steels, characterised by a distinct, hard, and brittle layer [20]. It appears as a white band under optical microscopy due to its resistance to chemical etching. WEL formation in rails is typically attributed to severe plastic deformation and/

* Corresponding authors.
E-mail addresses: zhang.tudelft.994@gmail.com (P. Zhang), z.li@tudelft.nl (Z. Li).

https://doi.org/10.1016/j.ijfatigue.2026.109620
Received 2 December 2025; Received in revised form 9 February 2026; Accepted 4 March 2026
Available online 6 March 2026

or thermal phase transformation resulting from cyclic wheel–rail friction rolling contact [21,22]. WEL has been considered as a potential initiator of RCF cracks due to its brittle nature [22–25]. Sometimes WEL is present together with a Brown Etching Layer (BEL). The BEL is a more recently identified surface layer [26], which appears brown after etching and is characterised by lower hardness compared to the WEL. The formation mechanism of BEL is not fully clear; it could be considered a tempered pre-existing WEL [22,27] or a precursor of the WEL [27,28].

The study in [29] reported that abusive grinding generated WEL on the heat-treated pearlitic rails and causes microcrack initiation under tangential wheel–rail contact stress, which may reduce the normal RCF life. A similar observation was made in [24], where a high density of cracks was found to originate at the interface between the softer pearlite matrix and the harder WEL, which is believed to be a direct consequence of the grinding. In [30], microstructural evolution and damage progression were investigated on a single-track railway line following preventive grinding. The findings indicated that the local damage mechanism is closely associated with the altered surface condition resulting from the grinding process. The work in [31,32] assessed the impact of grinding on surface quality and crack propagation in both twin-disc and field rail samples. It is found that grinding produced WEL across various rail grades, and harder grades retained larger quantities of WEL due to the smaller hardness gradient between the WEL and bulk material, which could promote the formation of cracks. However, the same study [31] also noted that the number of cracks does not have any significant differences between rail samples with and without WEL/grinding. In [33], the effect of rail grinding on RCF in conventional rail was examined, where it was concluded that grinding not only removes surface fatigue damage caused by repeated wheel–rail interaction but may also reduce subsurface stress concentrations, thereby potentially improving fatigue resistance.

Overall, there seems to be no clear consensus on the impact of grinding on mitigating or accelerating rail RCF. Moreover, most existing studies analyse the transient or short-term effect [29,34] and provide limited insight into the long-term consequences of grinding on rail degradation in field conditions. Some researchers explored the long-term evolution of rail surface damage after grinding under laboratory conditions [35–37]; they may not fully replicate the complexities of real-world rail operations.

To bridge this gap, the present study investigates the long-term impact of rail grinding on rail material evolution, particularly concerning WEL and RCF. Seven field rail samples with different grinding histories, accumulated tonnages, and steel grades were analysed. The samples were taken from the Belgian and Swedish railway networks; five of them underwent grinding passes according to the EN13231-3 standard series for the acceptance of reprofiling rails in track, while the remaining two were used as reference samples. The analysis includes microstructural characterisation and mechanical properties to assess the evolution of rail damage over time. Compared to the previous research [29–34], this work mainly focuses on the long-term post-grinding effect on in-service rail up to 31 MGT. The structure of this paper is as follows. Section 2 introduces the rail samples and microstructural investigation methods. Section 3 presents the results for six ground and unground samples from the Belgian railway network. Section 4 describes the microstructural findings from a Swedish rail sample after corrective grinding. Section 5 provides a discussion on the influence of grinding on rail damage evolution. Section 6 summarises the main conclusions of the study.

2. Methodology

This section provides an overview of the field conditions associated with six rail samples from the Belgian railway network and one sample from the Swedish network. Additionally, the sample preparation procedures and microstructural analysis methods are briefly described.

2.1. Rail samples on the Belgian railway network

Six rail samples were collected from two lines of straight tracks, L130B and L40 (see Fig. 1a and 1b), on the Belgian railway network, as listed in Table 1 and shown in Fig. 1c. The first four samples (R1–R4) were taken from Line L130B, with a traffic speed of 100 km/h and annual tonnage of 4 MGT. The remaining two samples (R5 and R6) were taken from Line L40, which has the same train speed but a higher annual load of 8 MGT. Samples R1 and R2 were manufactured from R260 steel grade, while R3 through R6 were made from R350. All rails followed the 60 E1 profile and conformed to CEN standard EN 13674–1.

These six rail samples experienced different loading and grinding histories, as detailed in Table 1. R1 was installed in March 2012, ground once in November 2018, and removed from service in December 2020. R2 and R3 were also installed in March 2012 but were never ground before being removed in December 2019. R4, installed in March 2012, underwent one grinding cycle in November 2018 and was removed in December 2019. R5 and R6 were both installed in May 2012. R5 was ground once in June 2015, while R6 was ground once in June 2015 and twice more in November 2018; both were removed from service in December 2019. In Belgium, each grinding cycle consisted of two grinding passes, with a total material removal of approximately 0.25 mm in accordance with EN 13231–3. The resulting longitudinal rail profile satisfied Class 2 requirements (EN 13231–3), while the transverse profile met Class R, Group B criteria with a deviation interval of 0.6 mm. The rail surface was continuously finished without visible bluing marks, and the maximum surface roughness was limited to 10 μm Ra, all acceptance criteria were met in accordance with EN 13231–3. The grinding train was equipped with 48 grinding stones (22–24 Ampère per stone), with the following chemical components of 36% Al_2O_3, 23% Zr, 4.8% Fe_2O_3, 4% F, 3.6% S, 1.6 K_2O, 1.5% SiO_2.

These rail samples were extracted from the field and transferred to Infrabel's laboratory for analysis. For five of the six samples (R2–R6), both longitudinal and transverse cross-sections were prepared and examined using etched optical microscopy (OM). Due to its limited longitudinal thickness, only the transverse section was analysed for Sample R1. All cross-sections were observed around the centre of the running band, corresponding to the primary wheel–rail contact zone. Additionally, surface hardness was measured to support the microstructural evaluation using the Vickers hardness method with a test load of 1 kg, in accordance with NBN EN ISO 6507–1. Five hardness measurements were performed at the middle of the running band along the rolling direction, see an example on R6 in Fig. 1c. Overall, this dataset provides a basis for evaluating the long-term impact of rail grinding on material degradation and damage mechanisms. Besides, it allows for the investigation of other relevant influencing factors such as steel grade and traffic load.

2.2. Rail sample on the Swedish railway network

One rail sample was collected from Line 414 of the Swedish railway network with a traffic speed of 180 km/h, as shown in Fig. 2a. The rail, made of R260 with a 50 E3 profile, was installed in a curve with a radius of 1000 m in 1974 and has been subjected to an annual traffic load of 13 MGT. In Sweden, standard preventive rail grinding typically involves 4–5 passes, removing 0.3–0.5 mm of material from the rail head. However, in 2020, an extended grinding operation was carried out on Line 414 to reprofile the rail and fully remove head checks. This procedure involved 30–35 grinding passes, resulting in a total material removal of approximately 5–6 mm. This rail sample from the high rail was removed from service in 2021, around one year after the grinding. Taking into account both artificial wear from grinding and natural wear from service, the total vertical wear of the sampled rail reached approximately 11 mm.

A transverse cross-section of the rail was prepared by wet cutting, polishing, and etching for detailed microstructural analysis, as shown in

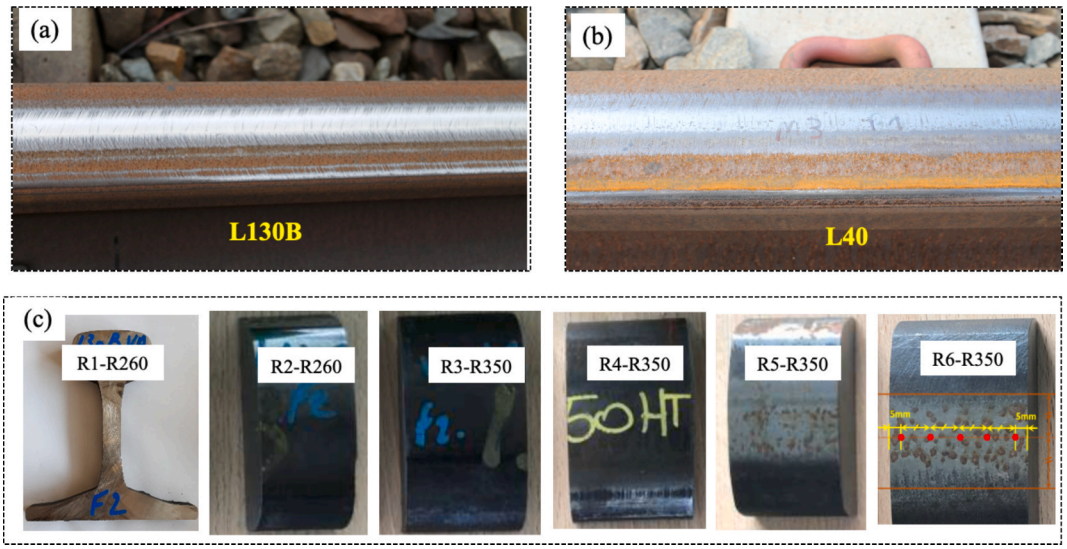

Fig. 1. Six rail samples taken from two straight lines in Belgium. (a) Track segment on Line 130B after one grinding cycle; (b) track segment on Line 40 after one grinding cycle; (c) six rail samples R1 to R6 in the laboratory. The five red points on R6 indicate the surface hardness measurement locations.

Table 1
Six field rail samples from the Belgian railway network.

Rail sample	Line	Radius	Speed (km/h)	Rail profile	Steel grade	Annual load	Installation	Grinding	Out of track
R1	L130B	∞	100	UIC60E1	R260	4 MGT	2012–03	2018–11	2020–12
R2	L130B	∞	100	UIC60E1	R260	4 MGT	2012–03	none	2019–12
R3	L130B	∞	100	UIC60E1	R350	4 MGT	2012–03	none	2019–12
R4	L130B	∞	100	UIC60E1	R350	4 MGT	2012–03	2018–11	2019–12
R5	L40	∞	100	UIC60E1	R350	8 MGT	2012–05	2016–05	2019–12
R6	L40	∞	100	UIC60E1	R350	8 MGT	2012–05	2016–05& 2018–11	2019–12

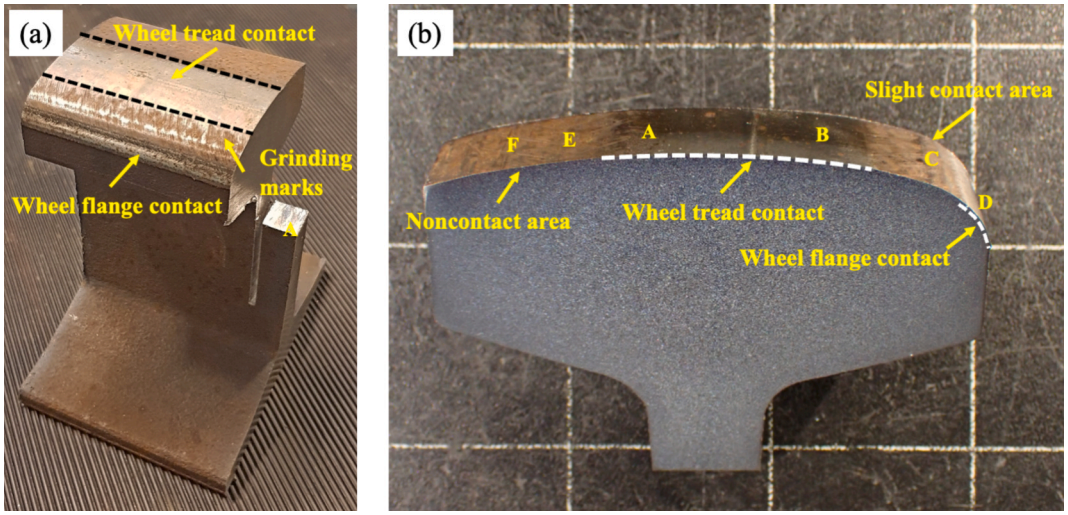

Fig. 2. The rail samples collected from the Swedish railway network. (a) The rail sample; (b) the prepared cross-section for microstructural analysis.

Fig. 2b. Based on observations and surface features, the rail head was divided into four distinct zones: 1) the wheel tread–rail head contact zone (Positions A, B), 2) the wheel flange–rail gauge contact zone (Position D), (3) a slight contact region on the rail shoulder (Position C) with residual grinding marks (see Fig. 2a), and (4) a non-contact area (Positions E, F). The examination was conducted using OM and scanning electron microscopy (SEM) at these zones across the rail head. Microhardness tests were performed using Vickers indentation from the rail surface to a depth of 10 mm. The prepared rail sample was used to examine the microstructure at various positions around the rail head and the presence of surface defects, such as WEL or cracks.

3. Results of Belgian rail samples

3.1. Sample R1-R260 with one grinding cycle on Line 130B

Fig. 3 shows the OM images of the R260 rail microstructure at sample R1 on Line 130B, around 8 MGT after one grinding cycle, which are

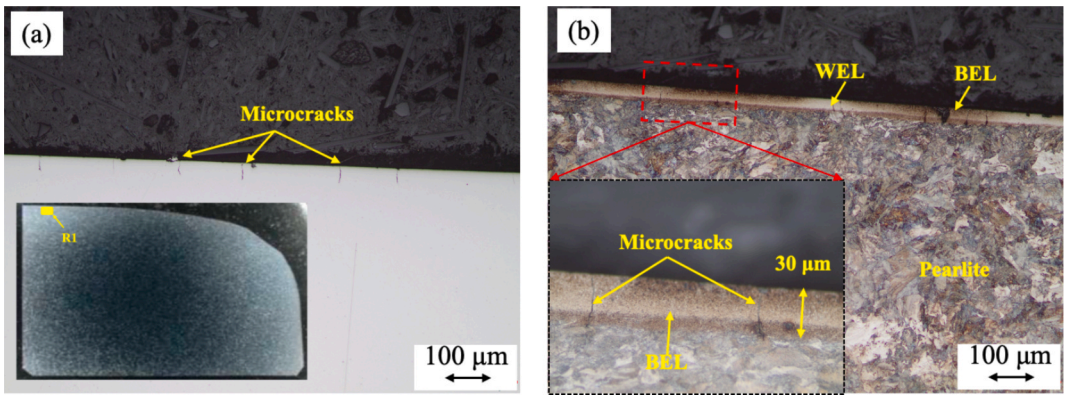

Fig. 3. The transverse cross-sections of Sample R1, R260 rail on Line 130B after one grinding cycle, (a) before etching, (b) after etching.

located approximately in the centre of the running band within the wheel–rail contact zone. The unetched image in Fig. 3a reveals that the rail running surface contains many fine, predominantly vertical cracks. After etching, a distinct layer comprising a mixture of WEL/BEL is observed in the proximity of the rail surface; it has a thickness of about 30 µm, as shown in Fig. 3b. Several microcracks are found to originate within this layer, and some are seen to penetrate through it and reach the boundary between the BEL and pearlitic microstructure, see the close-up in Fig. 3b. These could be attributed to the brittle nature of the WEL, which makes it prone to cracking under cyclic contact loading. These microcracks are similar to the observations in [25], which show multiple cracks propagating at an angle of ~ 90∘ to the surface within the WEL region.

The hardness values on the rail surface range from 307 to 389 HV, significantly exceeding the nominal hardness of R260 pearlitic steel, which is approximately 275 HV [38]. This increase is mainly caused by the work hardening and plastic deformation resulting from repetitive wheel–rail contact as well as rail grinding. They are lower than the typical hardness range reported for WEL/BEL, and likely represent a combined response of the near-surface material, including the rail pearlitic matrix and any thin WEL/BEL present. No pronounced plastic deformation is observed in the subsurface, which may be related to the observation location on a straight track where lateral wheel–rail interaction is limited.

3.2. Sample R2-R260 without grinding on Line 130B

Fig. 4 shows OM images of the R260 rail microstructure at Sample R2, which had not undergone any grinding. The unetched image (Fig. 4a and 4c) reveals an irregular rail head surface characterized by small flaking and surface microcracks. After etching, a WEL layer is observed in the rail materials in Fig. 4b and 4d, with a thickness ranging from 5 to

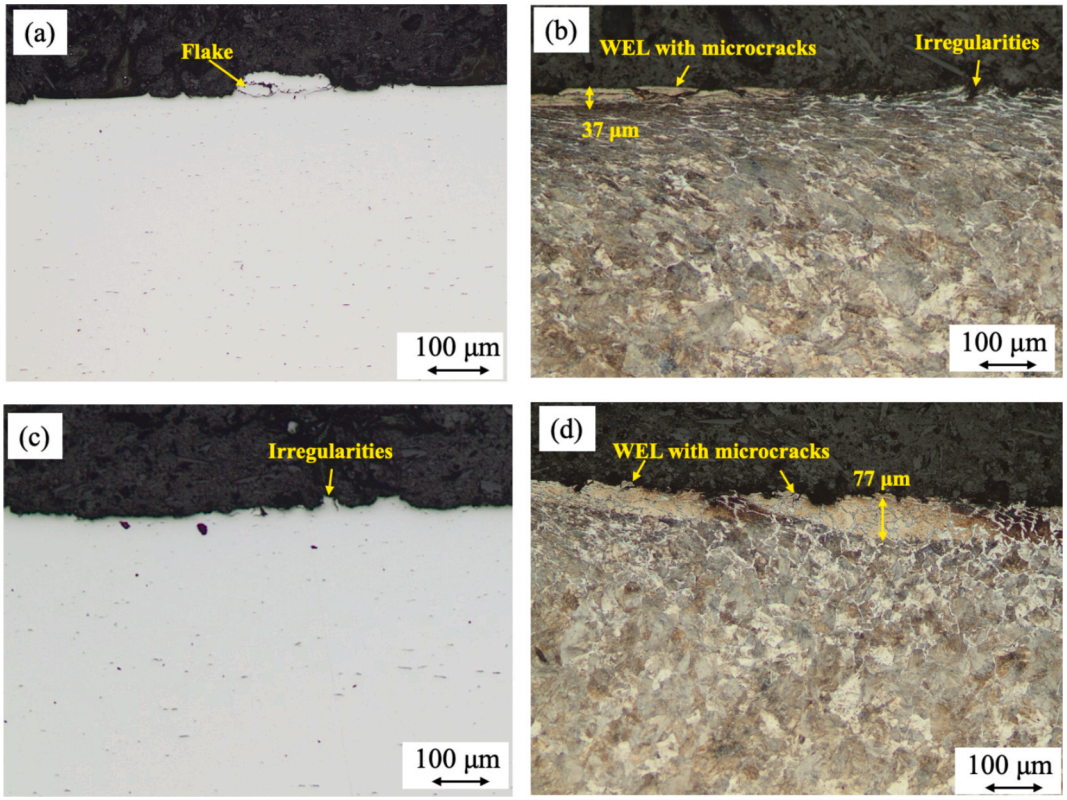

Fig. 4. The OM images of Sample R2, R260 rail on Line 130B without grinding, (a) Longitudinal cross-section before and (b) after etching; (c) transverse cross-section before and (d) after etching.

77 μm. Additionally, severe plastic deformation is observed in the near-surface region of Fig. 4b with depths of approximately 200–300 μm. Given the substantially higher accumulated tonnage (~31 MGT) and the absence of grinding, the WEL is more likely associated with severe plastic deformation–induced microstructural transformation (mechanical WEL) rather than a thermal WEL [22,39]. The rail surface hardness of R2 ranges from 343 to 394 HV, comparable to and slightly higher than those of Sample R1.

A comparison of Figs. 3 and 4 indicates that the ground (R1) and unground (R2) samples both have a WEL/BEL layer with thicknesses up to several tens of micrometres, accompanied by microcracks and increased surface hardness. This result suggests that the single grinding cycle performed on R1 did not introduce macrocracks and therefore did not adversely affect the surface integrity during long-term service. In addition, R1 displays a smoother surface than R2, likely as a result of the grinding process. The similar hardness values between R1 and R2 imply that the surface hardening of R260 rail steel may reach a saturation point after approximately two years of service (R1, ~8 MGT). Notably, no macrocracks were observed in the R260 rail (R2) after 7 years and 9 months of service (~31 MGT), indicating good resistance of R260 steel to RCF under the examined conditions. In this work, macrocracks refer to the relatively large cracks that typically propagate into the bulk materials and deeper than 0.1 mm [19].

3.3. Sample R3-R350 without grinding on Line 130B

Fig. 5 shows OM images of the R350 rail microstructure at Sample R3, which had not been subjected to grinding. The unetched images (Fig. 5a and 5c) reveal a highly irregular rail surface with many flakes. Notably, both microcracks and macrocracks are present in this sample. For instance, the crack shown in Fig. 5a extends to a depth of 68 μm and a length of 280 μm, oriented at an angle of 11° relative to the rail surface in the longitudinal cross-section. In Fig. 5c, four cracks are visible, with depths reaching up to 133 μm and an orientation angle of approximately 30° in the transverse cross-section.

Post-etching images (Fig. 5b and 5d) show the presence of a WEL near the rail surface, with thicknesses ranging from 5 to 45 μm. Unlike Samples R1 and R2, where microcracks are confined to the brittle WEL/BEL layer, Sample R3 has macrocracks that propagate deeply into the underlying pearlitic microstructure. Besides, these cracks are observed to initiate at discontinuities in the WEL, either at layer breakages or at the interface between the WEL and the pearlitic material, as highlighted by the red dashed ovals. The surface hardness ranges from 528 to 988 HV, indicating significant surface hardening and confirming the presence of the WEL.

In comparison to Sample R2 (R260 rail), the R350 rail appears to exhibit lower resistance to RCF under the examined conditions (~31 MGT), as evidenced by the presence of deeper and more severe cracks. Similar observations have been reported in [29,32].

3.4. Sample R4-R350 with one grinding cycle on Line 130B

Fig. 6 shows OM images of the R350 rail microstructure at the centre of the running band of Sample R4, where one grinding cycle had been performed. The unetched image in Fig. 6a shows a relatively smooth surface with few microcracks. After etching (Fig. 6b), the WEL layer becomes visible, with a thickness ranging from 5 to 35 μm. The underlying pearlitic grains show slight plastic deformation, and no macrocracks are observed. The surface hardness is between 449 and 697 HV, much smaller than that of R3.

In comparison to Sample R3 (unground R350), Sample R4, after one year of service following a grinding cycle (~4 MGT), has significantly fewer microcracks, the absence of macrocracks, a smoother surface, and lower surface hardness. These observations suggest that rail grinding has a beneficial effect on the resistance of R350 rails to RCF by removing the pre-existing plastic deformation layer and initial cracks.

3.5. Sample R5-R350 with one grinding cycle on Line 40

Fig. 7 presents OM images of the R350 rail microstructure at Sample

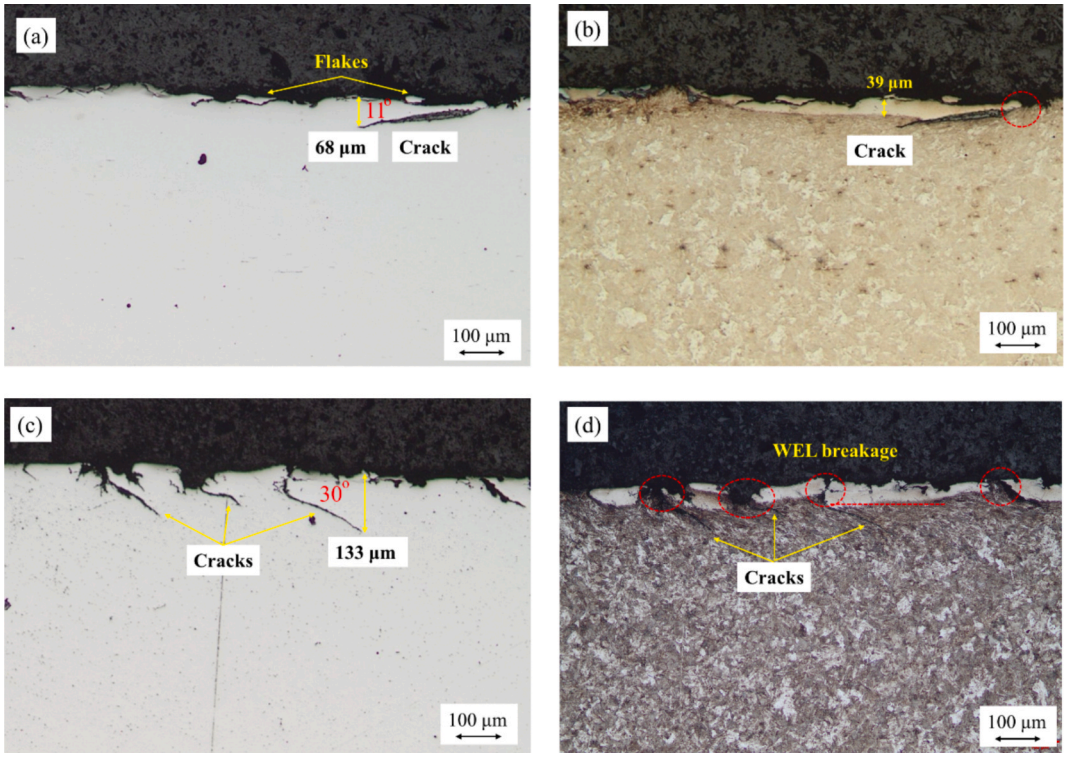

Fig. 5. The OMs of Sample R3, R350 rail on Line 130B without grinding. (a) Longitudinal cross-section before etching; (b) longitudinal cross-section after etching; (c) transverse cross-section before etching; (d) transverse cross-section after etching.

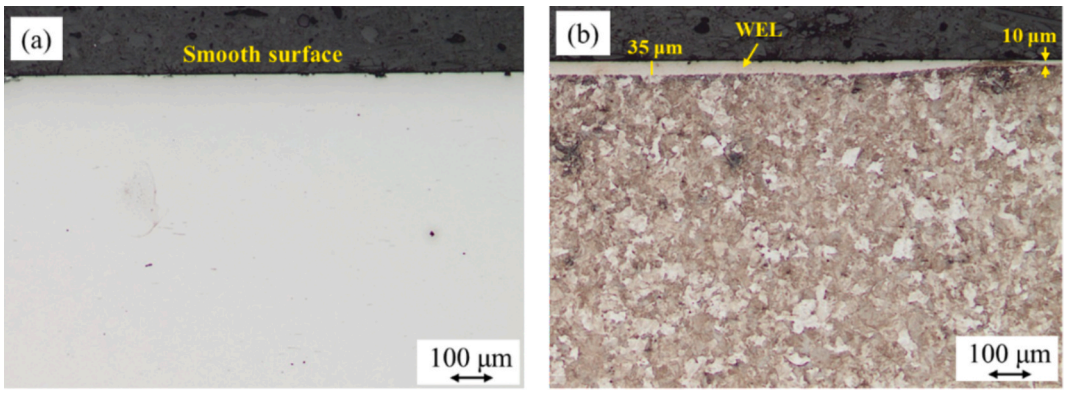

Fig. 6. The longitudinal cross-sections of Sample R4, R350 rail on Line 130B after one grinding cycle, (a) before etching, (b) after etching.

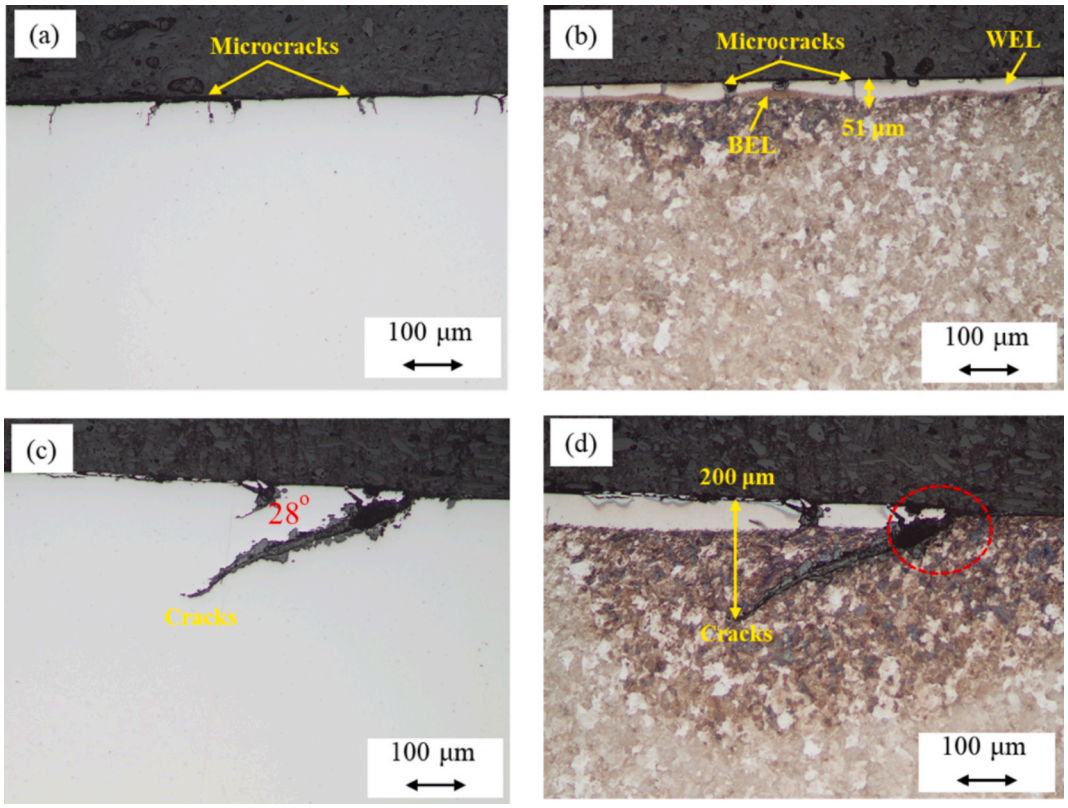

Fig. 7. The OMs of Sample R5, R350 rail on Line L40 with one grinding. (a) Longitudinal cross-section before etching; (b) longitudinal cross-section after etching; (c) transverse cross-section before etching; (d) transverse cross-section after etching.

R5, taken from the other track, Line 40, after one grinding cycle. The unetched images (Fig. 7a and 7c) show numerous microcracks as well as some macrocracks on the running surface. In particular, Fig. 7c shows a prominent crack reaching a depth of approximately 200 µm, with an orientation angle of 28° relative to the surface, similar to the angle observed in Sample R3. The grey material observed inside the crack is likely oxide debris formed during repeated crack opening and closing under rolling contact [6], which allows oxygen and moisture to ingress, particularly in an open-track environment.

After etching (Fig. 7b and 7d), a mixture of WEL/BEL is observed, with a thickness ranging from 20 to 80 µm. The microcracks are seen to initiate within this layer and propagate into the interface of the underlying pearlitic structure. The macrocracks are predominantly located at the transition between the WEL and the pearlite. Surface hardness ranges from 470 to 948 HV, which is similar to the values recorded for Sample R3.

Despite differences in railway lines and total accumulated loads (around 61 MGT for R5 and 31 MGT for R3), both the ground Sample R5 and the unground Sample R3 exhibit macroscopic cracks with comparable orientations and similar ranges of surface hardness. A closer analysis reveals that both samples experienced a similar post-grinding load: approximately 29 MGT for R5 and 31 MGT for R3 (without grinding), suggesting that accumulated tonnage after grinding is a more relevant parameter than total service tonnage when assessing RCF development.

3.6. *Sample R6-R350 with two grinding cycles on Line 40*

Fig. 8 shows OM images of the R350 rail microstructure at Sample R6, which had undergone two grinding cycles. The unetched image (Fig. 8a) shows the presence of corrosion products near the surface, along with minor surface flakes and microcracks. After etching (Fig. 8b),

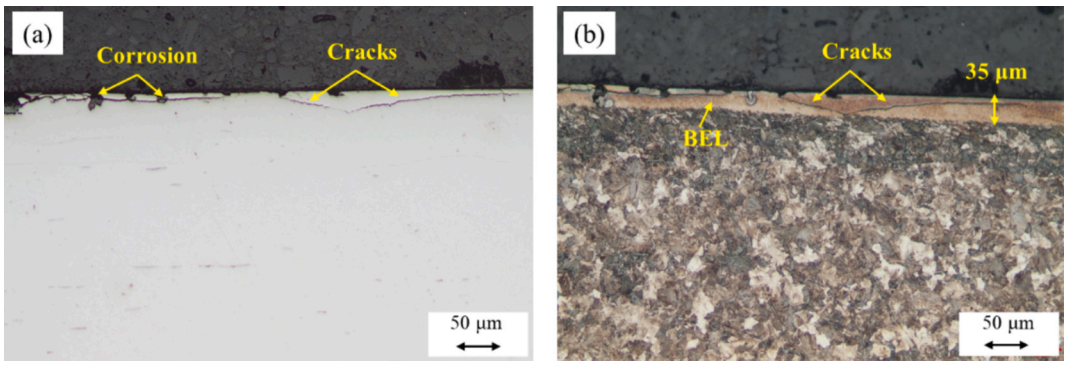

Fig. 8. The OMs of Sample R6, R350 rail on Line 40 with two grinding cycles. (a) Longitudinal cross-sections before etching; (b) longitudinal cross-sections after etching.

a BEL is observed in the rail material, with a thickness ranging from 10 to 40 μm. Relatively long cracks are seen to initiate within this layer, either parallel to the surface or propagate with a shallow angle and stop at the interface of the underlying pearlitic microstructure. The surface hardness values range from 564 to 734 HV.

Compared to Sample R5, Sample R6 has no macrocracks penetrating into the pearlite, but some microcracks confined within the BEL layer. The lower surface hardness may result from a combination of reduced accumulated plastic deformation and the absence of a hard WEL, with the near-surface region being dominated by BEL.These observations indicate that the second grinding cycle performed on R6 had a beneficial effect in removing pre-existing damage layers and enhancing resistance to RCF cracks. Additionally, the surface hardness of R6 is comparable to and slightly higher than that of Sample R4, which may be attributed to their relatively low post-grinding loads, approximately 9 MGT for R6 and 4 MGT for R4, significantly less than the loads for Samples R3 and R5. This further supports the hypothesis that post-grinding load is more relevant in determining surface condition and RCF development.

3.7. Summary of samples R1-R6

Table 2 provides a summary of the microstructural observations for all the six rail samples from the Belgian railway network. Regardless of grinding history, all samples show the presence of WEL and/or BEL, accompanied by microcracks and surface flaking. The thickness of these surface layers ranged from 5 to 80 μm, and grinding does not introduce macrocracks and therefore did not adversely affect the surface integrity during long-term service.

A comparison of rail samples (R3–R6) subjected to increasing post-grinding tonnage (4, 9, 29, and 31 MGT) reveals a trend of progressively accelerated damage evolution with increasing service loads. Macrocracks were identified only in Samples R3 and R5, while Samples R4 and R6, which had the same materials and loads but underwent more frequent grinding cycles, present no macrocracks. This suggests that rail grinding enhances the resistance of R350 to RCF by effectively removing the damaged layers. High surface hardness values were recorded in both R260 and R350 rail steels, especially in regions containing WEL, confirming the brittle nature. Samples with more grinding cycles generally exhibited lower surface hardness, implying that grinding helps remove the accumulated plastic deformation layers. In addition, ground samples show smoother surfaces in OM images and fewer surface irregularities than unground ones.

In addition to microstructural analysis, statistical data from the Belgian rail network further demonstrate the effectiveness of preventive grinding. In 2015, approximately 2,500 ultrasonic defects were detected annually, a number that had declined to around 1,000 by 2023 following the implementation of preventive grinding programs. Similarly, the total length of track sections with small RCF defects (<5 mm), as detected via Eddy Current Testing, decreased from 400 km in 2015 to roughly 100 km in 2024 [11]. Across all six samples, the maximum depth of WEL/BEL layers and associated cracks was less than 0.2 mm. In Belgium, each grinding cycle removes approximately 0.25 mm of material from the rail surface. These routine grinding operations appear to be effective in fully removing early-stage RCF damage and maintaining rail surface integrity.

4. Results of the Swedish rail sample

This section presents the microstructural cross-section results of the Swedish rail sample. This sample has undergone a corrective rail grinding with a material removal of 5–6 mm, and was taken from the track after 1 year of service (~11 MGT).

4.1. Microstructural features within the wheel-rail contact zone

Fig. 9 shows the OM images of the R260 rail microstructure in the wheel tread-rail head contact zone at two positions, A and B (see Fig. 2). It can be seen that a continuous WEL/BEL layer was present at Position A with a thickness of about 20–60 μm, while at Position B the WEL is discontinuous and appears as small patches together with an underlying BEL. Cracks and voids oriented nearly parallel to the rail surface are also visible, although they do not appear to propagate into the underlying pearlitic structure. The micro-hardness at both locations was about 280–290 HV near the rail surface, and reduced to 235–245 HV at a depth of 10 mm. Within the WEL, localised hardness values reach as high as 830 HV. It is observed that position B contains a thicker BEL and a much

Table 2
Microstructural observations of six field rail samples from the Belgian railway network.

Sample	Grinding cycles	Total load(MGT)	Post-grinding load(MGT)	WEL/ BEL (μm)	Hardness (HV)	Micro cracks	Macro cracks	Surface
R1	1	35	8	20–40	305–379	Yes	No	Smooth
R2	0	31	31	5–77	343–394	Yes	No	Irregular
R3	0	31	31	5–45	528–988	Yes	Yes	Irregular
R4	1	31	4	5–35	449–697	Yes	No	Smooth
R5	1	61	29	20–80	470–948	Yes	Yes	Smooth
R6	2	61	9	10–40	564–734	Yes	No	Smooth

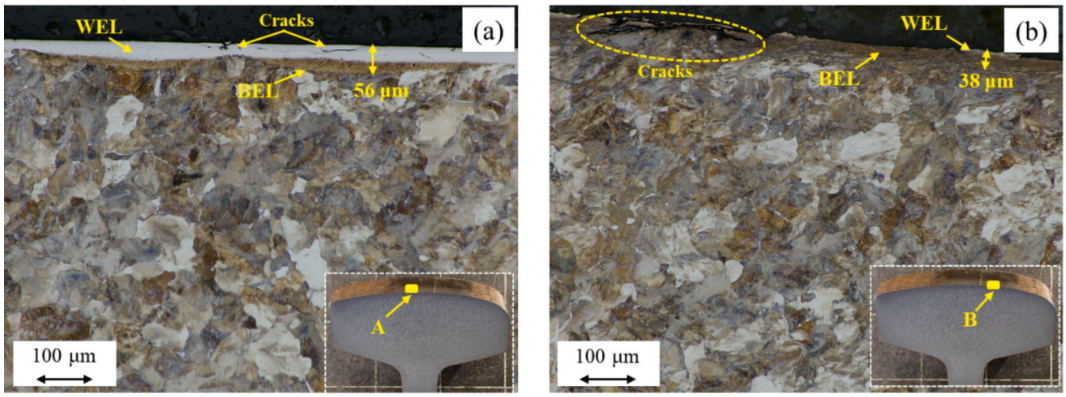

Fig. 9. The OM images of the Swedish rail sample in wheel tread-rail head contact zone. (a) Position A; (b) Position B.

thinner WEL compared to position A. Moreover, the cracks at position B are longer and penetrate more deeply, suggesting a larger local wheel-rail contact stress. It is also noted that the boundary between the BEL and the underlying plastic deformation layer cannot be clearly distinguished due to their similar contrast in the current optical micrographs; further analysis using higher magnification or SEM would be required to observe this boundary more clearly.

Fig. 10 presents the SEM images of this rail sample at position B for a more detailed examination. It can be seen from Fig. 10a that the rail surface shows signs of degradation after around 11 MGT of service, including peeling, spalling and small cracks. These cracks have a depth of dozens of micrometres, are nearly parallel to the surface, and stay within the surface WEL/BEL, as shown in Fig. 10b. Notably, no head checks or other defects were observed in this region of the sample, as shown in Fig. 2.

Fig. 11 shows OM images of the R260 rail microstructure at two locations: the slight contact region on the rail shoulder (Position C) and the wheel flange–rail gauge contact zone (Position D). As shown in Fig. 11a, the rail surface at Position C contains a thin and discontinuous WEL, with a thickness ranging from 5 to 15 μm. This region also exhibits signs of slight plastic deformation and an irregular surface profile, probably resulting from the grinding. In contrast, the microstructure at Position D (Fig. 11b) reveals a much smoother surface, which should be caused by more intense and consistent wheel–rail sliding contact. This area shows pronounced plastic deformation, a relatively thick BEL, and only limited WEL presence, similar to the characteristics observed in Fig. 9b. A small surface crack is observed in this region, approximately 43 μm in length. The micro-hardness at both locations was about 285 HV near the rail surface.

4.2. Microstructural features of the non-contact zone

Fig. 12 shows the OM images of the R260 rail microstructure in the non-contact zone at two positions, E and F. A discontinuous WEL is observed near the rail surface, with a maximum thickness of approximately 20 μm. In some areas, the WEL is absent, as shown in Fig. 12b. The rail surface has some irregularities, similar to those in Fig. 11a, probably introduced by the grinding. Microhardness measurements near the surface at both positions range from 280 to 290 HV, about 15% higher than the hardness measured at a depth of 10 mm, indicating that grinding has induced a certain degree of plastic deformation and surface hardening.

Compared to the contact zones shown in Fig. 9, the WEL in the non-contact zone (Fig. 12) is thinner, less continuous, and associated with fewer microcracks and with a more irregular surface. The overall hardness values are comparable in both cases. Additionally, the microstructural characteristics observed in the slight-contact region (Fig. 11a) closely resemble those in Fig. 12a, confirming minimal contact in that area.

5. Discussions

Two primary mechanisms have been proposed for RCF crack initiation in the rail surface: the ratcheting (I) [40–42] and WEL (II) mechanisms [29,43]. Crack initiation may occur due to high stress cyclic contact between the wheel and rail, which leads to progressive accumulation of plastic strain or ratcheting (Mechanism I) of rail materials and eventually exhaustion of ductility. Cracks typically initiate at the surface and grow in the direction of maximum shear stress. In this process, the presence of WEL is not necessary [4,44]. An alternative hypothesis suggests WEL can act as an initiator for rail cracks due to its

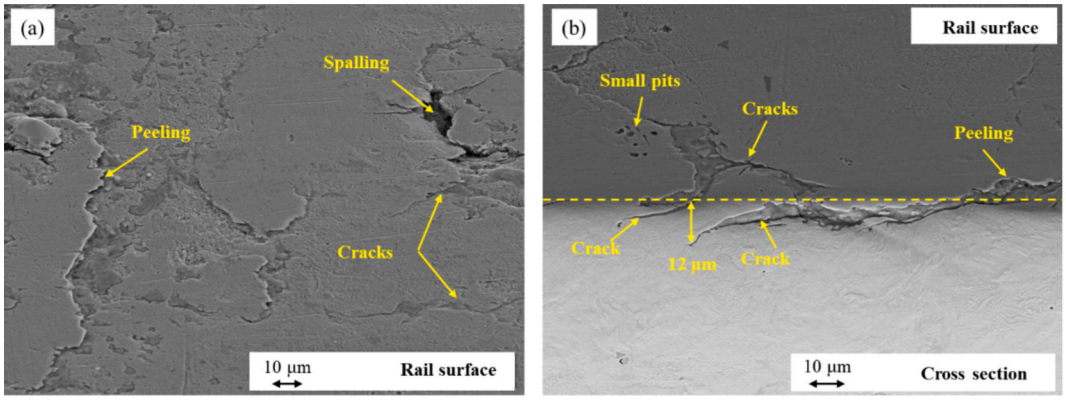

Fig. 10. The SEM images of the Swedish rail sample at position B. (a) on the rail surface; (b) a combination of the rail surface and cross section.

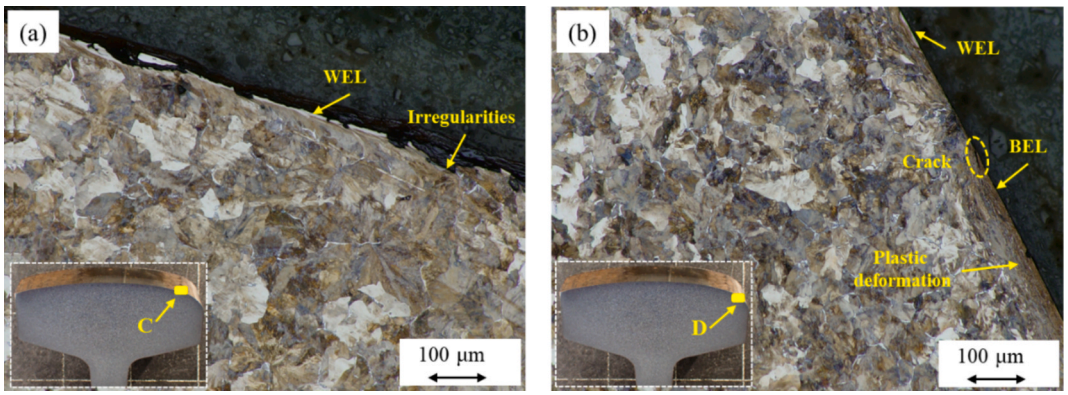

Fig. 11. The OM images of the Swedish rail sample in the wheel flange-rail gauge zone. (a) A slight contact region on the rail shoulder, Position C; (b) the wheel flange–rail gauge contact zone, Position D.

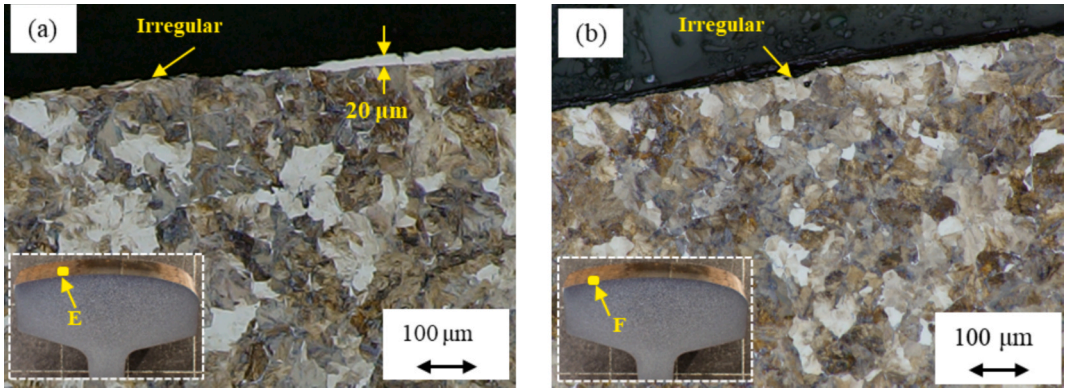

Fig. 12. The OM images of the Swedish rail sample in the non-contact zone. (a) Position E; (b) Position F.

hard and brittle nature (Mechanism II). WEL is prone to fracturing under wheel–rail contact stresses, and the resulting cracks can then propagate from the WEL into the soft underlying bulk material [43]. Moreover, the significant hardness gradient may promote localised stress concentrations at the interface, which promotes crack initiation [32].

Rail grinding removes the accumulated plastic deformation in the rail materials (see Fig. 4b), which may also eliminate early-stage cracks, thereby significantly reducing the likelihood of crack initiation via Mechanism I (ratcheting). However, the grinding process itself can generate the WEL and induce localised plastic deformation due to the high friction and temperature rise, as shown in Fig. 12 and reported in [24,29,32], which may, in turn, promote crack initiation via Mechanism II.

The comparison among the six rail samples from the Belgian rail network shows that both ground and nonground rail samples exhibit microcracks and WEL/BEL with depths of several tens of micrometres, as listed in Table 2. However, macrocracks were observed only in samples that had not been ground (R3) or had undergone fewer grinding cycles (R5). In addition, statistical data from the Belgian network show a significant reduction in the occurrence of RCF cracks following the implementation of preventive grinding. These findings highlight the beneficial role of rail grinding in mitigating RCF crack formation, and support that ratcheting is the dominant crack initiation mechanism under the examined conditions. The presence of WEL may also contribute to crack formation since macrocracks predominantly occur at the transition between the WEL and the pearlite.

In both the ground and nonground samples, many microcracks were observed within the WEL/BEL layers (see Table 2), a feature also identified in newly ground rails, as shown in Fig. 12 and [29]. Statistical data presented in [19] indicate that most microcracks do not evolve into macrocracks, likely due to the protective compressive stresses and their subsequent removal by wear. Therefore, grinding-induced microcracks may also be worn away before sufficient plastic deformation accumulates from wheel passages to drive further crack propagation. This could also explain why the R350 exhibits lower RCF resistance than R260 under identical loading conditions in this work. R350 material is harder and more wear-resistant than R260, which inhibits the removal of surface-initiated cracks. Similar findings have been reported in [32], where harder rails may be more susceptible to RCF damage.

In this work, all seven rail samples exhibit either WEL, BEL, or a combination of both (often referred to as a stratified layer in the literature). The formation mechanisms of WEL have been extensively studied and are generally attributed to mechanical or thermo-mechanical loading [21,25,45]. Recently, increasing attention has also been given to the formation mechanism of BEL. For example, the BEL in a pearlitic R350HT rail from service has been investigated in [28], which suggested a correlation between cementite decomposition and BEL formation. Detailed characterisation of the WEL and the BEL in a pearlitic rail steel has been carried out from micrometer to atomic scale in [27], and it is reported that BEL could be considered a tempered pre-existing WEL or a precursor of the WEL, depending on the time and peak temperature. Under well-controlled laboratory conditions, WEL/BEL have also been reproduced using defined mechanical loading combined with successive two thermal inputs [25,46], and it is found that the initial deformation state plays a critical role in determining the resulting microstructural characteristics of thermally induced WELs. While the present work is not intended to identify the formation mechanisms of WEL or BEL, some insights can be drawn from the field observations. In the investigated samples, predominantly WEL was observed in rails without grinding (Samples R2 and R3) or in non-contact zones subjected only to grinding

(Swedish sample), whereas BEL was mainly observed in regions exposed to the combined effect of subsequent wheel–rail contact loading and grinding. Further studies could be performed to fully clarify these observations.

Rail grinding introduces initial surface roughness by residual grinding marks, which are gradually smoothed out through wheel–rail interaction over time [34,47]. This explains the smoother surface observed in the OM images of the ground rail samples than in the unground ones in Section 3. However, if pre-existing cracks are too deep to be fully removed by grinding, the resulting surface roughness and local high contact stresses may accelerate crack growth, as reported in [11]. Therefore, it is essential to optimise grinding operations, such as selecting appropriate grinding stone materials and minimising friction during grinding, to reduce initial surface roughness and limit the formation of WEL/BEL and plastic deformation. It is worth noting that the results obtained in this study are achieved by grinding in certain methods and the influence of grinding parameters needs to be further investigated.

6. Conclusions

This study evaluates the long-term effects of grinding on rail material degradation through microstructural analysis of seven in-service rail samples. Six of them were selected from straight track sections of the Belgian rail networks, and the other from the high rail in a 1000 m radius curve in the Swedish railway network. These samples have different grinding operations, steel grades and load histories, and their mechanical and microstructural properties were examined via the hardness test, OM, and SEM. The main findings have been summarised as follows.

(1) WEL and microcracks were observed in both ground and non-ground rails among the seven investigated samples, suggesting that rail grinding may not introduce additional defects or adversely affect the rail surface after long-term service.
(2) With identical materials and loads, macrocracks were observed only in rail samples that had undergone zero or a single grinding cycle in accordance with EN 13231 standard series. Besides, the statistical data show a considerable reduction in cracks of the Belgian railway network after the implementation of preventive grinding. These results confirm the beneficial role of rail grinding in mitigating RCF crack formation by removing the accumulated plastic deformation.
(3) Ratcheting is the dominant crack initiation mechanism under the examined conditions, while WEL may also contribute to crack formation, given that macrocracks predominantly occur at the transition between the WEL and the pearlite.
(4) Despite the initial WEL and local deformation, rail samples with more grinding cycles generally exhibited lower surface hardness after long-term service.
(5) Rail grinding introduces initial surface roughness, which is gradually smoothed out through wheel–rail dynamic interaction over time [34,47], causing a smoother surface than in unground ones.
(6) Post-grinding load is more relevant than the total accumulated load in determining the rail surface condition and RCF development.
(7) Under the examined service conditions, R260 steel demonstrated better resistance to RCF than R350, likely due to its higher wear rate, which facilitates the removal of early-stage surface cracks before they further grow.

Overall, this research provides valuable insights into the formation mechanism and prevention of RCF cracks in rails. It should be noted that the conclusions are based on a limited number of rail samples and certain grinding methods, and a broader dataset would help to validate and strengthen these findings. Besides, it is observed that BEL only occurs in some samples and not others, which could be further investigated in future studies. Moreover, further research could be performed to optimise grinding operations to avoid aggressive grinding and minimise initial surface damage and roughness.

CRediT authorship contribution statement

Tim Vernaillen: Writing – original draft, Visualization, Validation, Methodology, Investigation, Formal analysis, Data curation, Conceptualization. **Pan Zhang:** Writing – original draft, Visualization, Supervision, Methodology, Investigation, Formal analysis. **Stefan Lundström Sveder:** Visualization, Resources, Investigation, Data curation. **Alfredo Núñez:** Writing – review & editing, Supervision, Project administration, Methodology, Conceptualization. **Rolf Dollevoet:** Writing – review & editing, Supervision, Resources, Project administration. **Zili Li:** Writing – review & editing, Validation, Supervision, Resources, Project administration, Methodology, Investigation, Formal analysis, Conceptualization.

Declaration of competing interest

The authors declare that they have no known competing financial interests or personal relationships that could have appeared to influence the work reported in this paper.

Acknowledgments

This work is partly supported by Infrabel and Trafikverket. The authors thank Dr. Fang Ren for the helpful discussion about the crack initiation mechanism in Section 5.

Data availability

Data will be made available on request.

References

[1] Magel, E.E., *Rolling contact fatigue: a comprehensive review*. 2011.
[2] Ekberg A, Åkesson B, Kabo E. *Wheel/rail rolling contact fatigue–Probe, predict, prevent*. Wear 2014;314(1–2):2–12.
[3] Deng X, et al. *Investigation of the formation of corrugation-induced rail squats based on extensive field monitoring*. Int J Fatigue 2018;112:94–105.
[4] Ren F, Yang Z, Li Z. *Experimental and numerical investigation into rolling contact fatigue crack initiation on the V-Track test rig*. Eng Fail Anal 2025;170:109206.
[5] Bogdański S, Lewicki P. *3D model of liquid entrapment mechanism for rolling contact fatigue cracks in rails*. Wear 2008;265(9–10):1356–62.
[6] Al-Juboori A, et al. *Evolution of rail surface degradation in the tunnel: the role of water on squat growth under service conditions*. Eng Fract Mech 2019;209:32–47.
[7] Al-Juboori A, et al. *Microstructural investigation on a rail fracture failure associated with squat defects*. Eng Fail Anal 2023;151:107411.
[8] Zhou Y, et al. *Modeling of rail head checks by X-ray computed tomography scan technology*. Int J Fatigue 2017;100:21–31.
[9] Shen Y, et al. *Evolution and formation mechanism of rail corrugation in high-speed railways involving the longitudinal wheel-track coupling relationship*. Sci China Technol Sci 2024;67(11):3612–25.
[10] Zhang P, et al. *Parametric investigation of railway fastenings into the formation and mitigation of short pitch corrugation*. Railway Eng Sci 2024.
[11] Vernaillen T, et al. *Statistical analysis and treatment method of head checks on the Belgian railway network*. Int J Fatigue 2025:109349.
[12] Chattopadhyay G, Reddy V, Larsson-Kråik PO. *Decision on economical rail grinding interval for controlling rolling contact fatigue*. Int Trans Oper Res 2005;12(6):545–58.
[13] Grassie SL. *Rolling contact fatigue on the British railway system: treatment*. Wear 2005;258(7–8):1310–8.
[14] Zoeteman A, Dollevoet R, Li Z. *Dutch research results on wheel/rail interface management: 2001–2013 and beyond*. Proc Inst Mech Eng, Part F: J Rail and Rapid Transit 2014;228(6):642–51.
[15] Mesaritis M, et al. *Rail surface integrity analysis in laboratory*. Procedia CIRP 2024;123:83–8.
[16] Lin B, et al. *Influence of grinding parameters on surface temperature and burn behaviors of grinding rail*. Tribol Int 2018;122:151–62.
[17] Zhang Z, et al. *Thermal model and temperature field in rail grinding process based on a moving heat source*. Appl Therm Eng 2016;106:855–64.

[18] He C, et al. *Infrared temperature measurement of wheel-rail frictional rolling contact with high slip ratios*. Case Stud Therm Eng 2025;73:106642.
[19] Dikshit V, Clayton P, Christensen D. *Investigation of rolling contact fatigue in a head-hardened rail*. Wear 1991;144(1–2):89–102.
[20] Zhang HW, et al. *Microstructural investigation of white etching layer on pearlite steel rail*. Mater Sci Eng A 2006;421(1–2):191–9.
[21] Wu J, et al. *Laboratory simulation of martensite formation of white etching layer in rail steel*. Int J Fatigue 2016;91:11–20.
[22] Nguyen BH, et al. *Tribological behaviors of two distinct classes of white etching layers on rail surface*. Wear 2023;532:205097.
[23] Seo J, et al. *Numerical stress analysis and rolling contact fatigue of White Etching Layer on rail steel*. Int J Fatigue 2011;33(2):203–11.
[24] Rasmussen CJ, et al. *Surface crack formation on rails at grinding induced martensite white etching layers*. Wear 2017;384:8–14.
[25] Freisinger M, et al. *Fatigue crack initiation in the presence of stratified surface layers on rail wheels*. Int J Fatigue 2023;177:107958.
[26] Li S, et al. *"Brown etching layer": a possible new insight into the crack initiation of rolling contact fatigue in rail steels?* Eng Fail Anal 2016;66:8–18.
[27] Kumar A, et al. *Microstructural evolution of white and brown etching layers in pearlitic rail steels*. Acta Mater 2019;171:48–64.
[28] Tung P-Y, et al. *Formation mechanism of brown etching layers in pearlitic rail steel*. Materialia 2022;26:101625.
[29] Steenbergen M. *Rolling contact fatigue in relation to rail grinding*. Wear 2016;356:110–21.
[30] Schotsman B, et al. *Microstructure evolution and damage development in the rails of a single-track railway line after preventive grinding*. Wear 2025;576:206101.
[31] Mesaritis M, et al. *A laboratory demonstration of rail grinding and analysis of running roughness and wear*. Wear 2020;456:203379.
[32] Mesaritis M, et al. *Post-field grinding evaluation of different rail grades in full-scale wheel/rail laboratory tests*. Tribol Int 2023;177:107980.
[33] Satoh Y, Iwafuchi K. *Effect of rail grinding on rolling contact fatigue in railway rail used in conventional line in Japan*. Wear 2008;265(9–10):1342–8.
[34] Edjeou W, et al. *Evaluating the impact of rail surface roughness post-grinding: an experimental and elastoplastic modelling approach*. Tribol Int 2025;201:110270.
[35] Wang R, et al. *Effects of abrasive material and hardness of grinding wheel on rail grinding behaviors*. Wear 2020;454:203332.
[36] Mesaritis M, et al. *Assessment of rail grinding maintenance surface quality and damage propagation in subsequent loading cycles for premium rail grades*. Wear 2023;530:205051.
[37] Uhlmann E, et al. *Influence of rail grinding process parameters on rail surface roughness and surface layer hardness*. Wear 2016;366:287–93.
[38] Zhang P, et al. *Microstructural investigation into the damage mechanism of short pitch rail corrugation*. Eng Fail Anal 2025;174:109512.
[39] Freisinger M, et al. *Severe plastic deformed zones and white etching layers formed during service of railway wheels*. Metall Microstruct Anal 2023;12(3):515–27.
[40] Tyfour W, Beynon J, Kapoor A. *Deterioration of rolling contact fatigue life of pearlitic rail steel due to dry-wet rolling-sliding line contact*. Wear 1996;197(1–2):255–65.
[41] Franklin F, et al. *Modelling rail steel microstructure and its effect on crack initiation*. Wear 2008;265(9–10):1332–41.
[42] Ren F, Yang Z, Li Z. *An efficient 3D finite element procedure for simulating wheel–rail cyclic contact and ratcheting*. Tribol Int 2024:109878.
[43] Al-Juboori A, et al. *Squat formation and the occurrence of two distinct classes of white etching layer on the surface of rail steel*. Int J Fatigue 2017;104:52–60.
[44] Pal S, Daniel WJ, Farjoo M. *Early stages of rail squat formation and the role of a white etching layer*. Int J Fatigue 2013;52:144–56.
[45] Nguyen BH, et al. *Fracture mechanisms in rails with mechanically and thermomechanically-induced white etching layers under three-point bending*. Eng Fail Anal 2022;131:105813.
[46] Freisinger M, et al. *Comparative study on the influence of initial deformation and temperature of thermally induced white etching layers on rail wheels*. Tribol Int 2023;177:107990.
[47] Zhang P, Li Z. *The development of short pitch rail corrugation: extensive field monitoring and validation of numerical predictions*. Tribol Int 2025:110821.